Numerical and experimental wind tunnel analysis of aerodynamic effects on a semi-submersible floating wind turbine response

Preprint of OMAE2019-95976 submitted to the 38th International Conference on Ocean, Offshore & Arctic Engineering, June 9-14, 2019, Scotland, Glasgow

A. Fontanella[1], I. Bayati [2], F. Taruffi[1], A. Facchinetti[1], M. Belloli[1]

[1]Mechanical Engineering Department, Politecnico di Milano, Milano, Via La Masa 1, 20156, Italy.
[2]Maritime Research Institute Netherlands (MARIN), Wageningen, 6708 PM, The Netherlands.

Author contact email: alessandro.fontanella@polimil.it

1   ABSTRACT

This paper presents the main results of an experimental campaign about the DeepCwind semi-submersible floating offshore wind turbine (FOWT), that was carried out at Politecnico di Milano wind tunnel, adopting a hybrid hardware-in-the-loop (HIL) testing technique. Differently from previous works by the authors, this further analysis herein reported, is specifically focused on evaluating the effects of aerodynamic loads on the FOWT platform motions. In order to reproduce the FOWT response to combined wind and waves in a wind tunnel, exploiting the high-quality flow, a HIL system was used. The aerodynamic and rotor loads were reproduced by means of a wind turbine scale model operating inside the wind tunnel and were combined with numerically generated wave loads for real-time integration of the FOWT rigid-body motion equations. The resulting platform motions were imposed to the wind turbine scale model by a hydraulic actuation system. A series of HIL tests was performed to assess the rotor loads effect on the FOWT response. Free-decay tests in still water under laminar un-sheared wind were carried out to evaluate how the aerodynamic forcefield modifies the platform modes frequency and damping. Irregular wave tests for different steady winds were performed to investigate the dependency of platform motion from the wind turbine operating conditions. A FAST v8 model of the studied floating system was developed to support the analysis and numerical simulations were performed to reproduce environmental conditions equivalent to those of the experimental tests. The FAST model prediction capability is discussed against HIL wind tunnel tests results.

2 NOMENCLATURE

DOF   Degree of freedom FOWT   Floating offshore wind turbine HIL   Hardware-in-the-loop PoliMi Politecnico Milano RWT   Reference wind turbine WTM   PoliMi wind turbine model f Motion frequency h Linear damping ratio H_s Significative wave height T_p Peak period U Hub-height mean wind speed x Platform surge displacement θ Platform pitch rotation

3 INTRODUCTION

Scale model testing has been recognized as an effective approach to investigate the complex physics of floating offshore wind turbines and to provide useful data for numerical models calibration and validation [27]. In particular, in the last years, hybrid hardware-in-the-loop (HIL) methodologies were developed in different laboratories to complement traditional ocean basin testing and overcome its intrinsic limitations [16]. When HIL testing is adopted, the floating system is divided into two main subsystems governed by different physics, that are modeled in the experiment either physically or numerically. In HIL ocean basin tests, measured platform displacements are fed to a numerical model of the wind turbine rotor and control system that is integrated in real-time to compute wind turbine loads. These are exerted on a physical scale model of the floating platform and wind turbine tower by means of an actuation system like tendons [26, 3], winches [21], a ducted fan [2, 28] or a multifan [5]. A complementary methodology was developed at PoliMi [14, 17] to study FOWTs dynamics exploiting the unique characteristics of PoliMi wind tunnel (Galleria del Vento Politecnico di Milano, GVPM [1]). Measured aerodynamic and rotor loads, that are reproduced by a physical wind turbine scale model, are combined with numerically computed hydrodynamic loads for real-time integration of the floating platform rigid-body motion equations. The resulting displacements are imposed to the wind turbine scale model by means of a proper actuation system.

By relying on a physical scale model to reproduce only part of the full-scale system, it is possible to investigate more deeply and at a lower uncertainty level the phenomena to which this is subjected. Great efforts were made at PoliMi to study the effects of unsteady rotor aerodynamic loads on the global FOWT response and, in particular on the platform surge and pitch DOFs. Aerodynamic loads were measured for different imposed sinusoidal motions [8, 12] and combined to a linear model [9] to understand how the aerodynamic forcefield affects the response of the platform rigid-body motion modes. Particle image velocimetry (PIV) and hot-wire measurements were recently performed [13, 6] to describe the flow field in the wind turbine wake and improve the understanding of unsteady rotor loads.

In this work, results of HIL wind tunnel tests about a floating system based on the OC5 DeepCwind platform [24, 25] are analyzed to understand how the platform surge and pitch DOFs response is influenced by wind turbine loads in three different operating conditions. The system object of experimental tests was also modeled in FAST v8.16 [23] and simulations equivalent to the experimentally simulated load cases were performed. HIL results are compared to simulations output to assess the prediction capability of FAST with respect to unsteady aerodynamics.

4 EXPERIMENTAL SETUP

The experimental setup adopted for the HIL wind tunnel test campaign object of this work (Fig. 1) is the same of [14, 17]. A brief description is reported here, whereas further details can be found in the above mentioned works.

The HIL system is composed of a rigid wind turbine scale model mounted on top of a hydraulic

Figure 1: 2 DOFs HIL set-up for hybrid wind tunnel tests.

Table 1: Scale factors for the HIL tests.

Factor	Expression	Value
Length	λ_L	$1/53$
Velocity	λ_v	$1/3$
Mass	$\lambda_M = \lambda_L{}^3$	$1/53^3$
Time	$\lambda_T = \lambda_L/\lambda_v$	$3/53$
Frequency	$\lambda_\omega = \lambda_v/\lambda_L$	$53/3$
Acceleration	$\lambda_a = \lambda_v/\lambda_L$	$53/3^2$
Force	$\lambda_f = \lambda_L^4/\lambda_T^2$	$1/(53^2 \cdot 3^2)$

actuation system. Tower base loads generated by the wind turbine scale model are continuously measured by a 6-components load cell (*RUAG 192-6I*). The sensor load reduction point is coincident with the ideal point where the wind turbine tower is connected to the floating platform. Wind turbine loads extracted from the load cell measurements are used for real-time integration of the floating platform equations of motion (EOMs). The resulting surge displacement (dynamic component only) and pitch rotation are imposed to the wind turbine model by the actuation system.

The most significative dimensions for the HIL experiments were scaled from the reference full-scale values according to the factors of Tab. 1. These were derived from dimensional analysis, after having independently set the length scale factor λ_L and velocity scale factor λ_v.

Wind turbine model

The wind turbine model (WTM) [11, 7], originally developed as a 1/75 scale model of the DTU 10MW RWT [4] within LIFES50+ project, is representative of a 1/53 scale model of the NREL 5MW [22] as explained in [17]. The wind turbine blades and tower can be considered rigid, since the

natural frequency of their first flexible modes are sufficiently above the wave excitation range. The model rotor was performance-scaled according to a specific design procedure [10] in order to match the RWT thrust and torque at the low-Reynolds conditions typical of wind tunnel tests.

HIL system

The platform surge and pitch response to hydrodynamic and wind turbine loads is computed from the real-time integration of the 2 DOFs floating platform equations of motion (EOM) of Eq. 1.

$$([M_s] + [A_\infty])\ddot{\underline{q}} + [R_s]\dot{\underline{q}} + [K_s]\underline{q} = \underline{F}_{plat} + \underline{F}_{wt} \tag{1}$$

where $[M_s]$ is the floating system (platform and wind turbine) mass matrix about the platform surge and pitch DOFs $\underline{q} = [x, \theta]^T$, $[A_\infty]$ is the infinite-frequency added mass matrix, obtained from 3D panel code (e.g. WAMIT) pre-computations. $[R_s]$ is adopted to introduce additional linear damping on the floating platform in order to match experimental data from ocean basin tests [24]. $[K_s]$ is the floating system gravitational and buoyancy stiffness matrix.

Floating platform loads $\underline{F}_{plat}$ are the sum of different contributions, summarized in Eq. 2, that are reproduced by an ad-hoc numerical hydrodynamic model.

$$\underline{F}_{plat} = \underline{F}_{rad} + \underline{F}_{we} + \underline{F}_{visc} + \underline{F}_{moor} \tag{2}$$

Radiation loads $\underline{F}_{rad}$, modeling the memory effect, are implemented exploiting the state-space approximation [19, 18] of the convolution integral between platform velocities and retardation matrix (impulse response) [14]. $\underline{F}_{we}$ are the first and second order wave excitation loads, $\underline{F}_{visc}$ the Morison's viscous loads and $\underline{F}_{moor}$ the loads exerted by the mooring system on the floating platform. Mooring line loads were implemented as pre-computed look-up tables as function of the surge position and pitch rotation. Thus, only the positional component of the mooring lines forces is kept into account in HIL experiments.

Wind turbine loads $\underline{F}_{wt}$ are obtained depriving of the inertial and gravitational components $\underline{F}_{corr}$ tower-base loads according to Eq. 3.

$$\underline{F}_{wt} = \underline{F}_{RUAG} - \underline{F}_{corr} \tag{3}$$

Wind turbine loads obtained according to Eq. 3 include the effect of aerodynamic rotor loads, aerodynamic tower loads, gyroscopic moments and mechanical rotor loads, whereas the reproduction of the inertial and gravitational components of wind turbine loads entirely relies on the numerical model.

Loads required to perform the force correction operations of Eq. 3 are defined as in Eq. 4, assuming the wind turbine model a single rigid-body moving in space.

$$\underline{F}_{corr} = [M_t]\ddot{\tilde{\underline{q}}}_a + [K_t]\tilde{\underline{q}}_a \tag{4}$$

Where $[M_t]$ and $[K_t]$ are the wind turbine model mass and gravitational stiffness matrix about the surge and pitch DOFs and $\tilde{\underline{q}}_a$ is the effective wind turbine surge and pitch motion as measured by the LVDTs sensors of the HIL actuation system.

Table 2: FAST/*AeroDyn 14* simulation settings.

Parameter	Setting
Dynamic stall	Steady (no dynamic stall)
Use C_m	No
Inflow model	Equil (no dynamic wake)
Induction factor model	Swirl
Tip loss model	Prandtl
Hub loss model	Prandtl

5 FAST SIMULATIONS VS HIL EXPERIMENTS

The HIL system is based on a simplified model of the floating system, designed to respect the performance constraints imposed by real-time integration. Nevertheless, the model should reproduce the platform response as best as possible the floating system dynamics as measured in still-air ocean basin tests.

To do this, a numerical model of the DeepCwind system used for ocean basin tests at MARIN [24] was created. The model is based on FAST, a high-order servo-aero-hydro-elastic simulation tool, and it is herein assumed as the reference representation of platform dynamics and hydrodynamic loads. The capability of the HIL system to reproduce platform dynamics in still air was then verified comparing experimental tests in no-wind conditions by means of equivalent FAST simulations. Differences between the output of FAST simulations and the outcome of HIL experiments are introduced due to the simplifications in the HIL numerical model and uncertainties in the HIL force feedback. The direct comparison of HIL experiments and FAST simulations highlights the combination of these differences, without the possibility of discerning single contributions. In previous works [14, 15, 17], uncertainties due to modeling choices and due to the HIL measurement and actuation chains were identified separately one from the others. For the sake of brevity, in this work, HIL results are compared directly to FAST outputs, whereas further details can be found in the referenced papers.

Once the capability of the HIL numerical model of reproducing platform dynamics and hydrodynamic loads is assessed, it is possible to consider the HIL system as the highest fidelity reproduction of the coupled servo-aero-hydro-elastic phenomena experienced by the full-scale wind turbine, at least for what concerns the aerodynamic component. HIL wind tunnel tests are then used as a benchmark for assessing the prediction capability of high-order numerical models with respect to the complete serovo-aero-hydro-elastic problem. In this work, the above-mentioned operation is performed for FAST v8.16/*AeroDyn 14*. A FAST model of the PoliMi setup was created combining the model of the DeepCwind platform and the model of the WTM rotor, implemented in emphAeroDyn 14 starting from the polars obtained for the airfoil of the different blade sections [10]. The *AeroDyn 14* settings used for all the simulations are reported in Tab. 2.

HIL verification - Free motion (no wind)

Free-motion tests were performed alternatively imposing an initial condition to the platform surge (+5.3 m) or pitch (+8°) DOF and allowing the system to come at rest. The surge and pitch dynamic response, obtained subtracting the static displacement from the overall motion, as resulting from HIL experiments and equivalent FAST simulation is shown in Fig. 2. Linear dynamic properties for the platform surge and pitch motion modes were computed from the analysis of the first 10
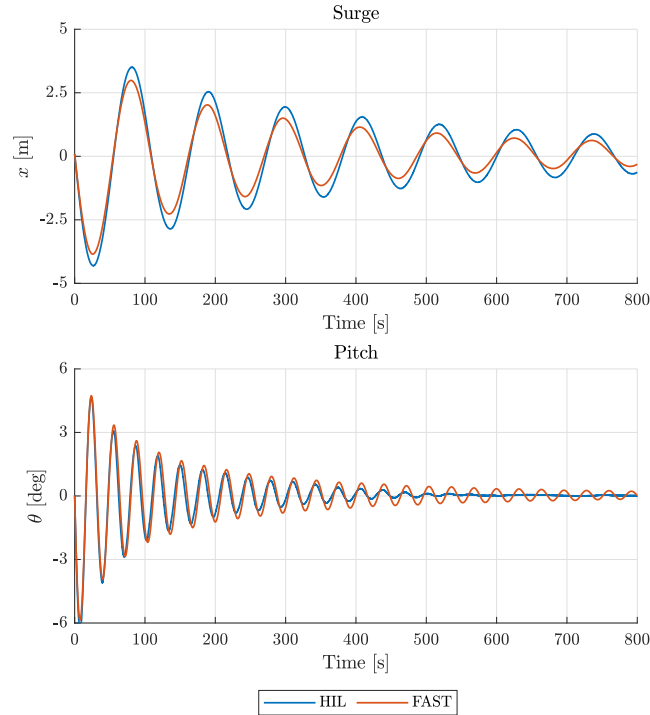
Figure 2: Platform surge and pitch dynamic response for a surge and pitch decays in still-air. Comparison between HIL tests and FAST simulations.

Table 3: Platform surge and pitch dynamic properties in still-air from HIL tests and FAST simulations.

	HIL		FAST	
U [m/s]	f [Hz]	h [%]	f [Hz]	h [%]
Surge	0.0092	0.0389	0.0093	0.0473
Pitch	0.0314	0.0426	0.0313	0.0374

oscillation cycles in the response of the DOF subjected to the initial condition. The motion frequency was detected from the FFT of the analyzed platform DOF response, whereas damping data were obtained applying the logarithmic decrement method. The surge and pitch motion frequencies and linear damping ratios from HIL tests are compared to those resulting from FAST simulations in Tab. 3 As visible, the surge mode response as reproduced in HIL tests is very close to what is predicted by the FAST model, with the latter showing a slightly higher damping than the first one. A slightly greater difference is seen for the pitch DOF, which damping from HIL tests is greater than in numerical simulations, especially at small oscillation amplitudes. The damping estimate from still-air HIL tests could be affected by the non-negligible dynamics of hydraulic actuators. Moreover, errors in the identified wind turbine model inertial parameters result in additional inertial and gravitational loads on the floating system that, in combination with actuation delays, are translated into an unphysical damping.

HIL verification - Irregular waves (no wind)

Irregular waves with 0° misalignment were run in order to assess the system response to stochastic broad-band excitation loads. Waves were generated during HIL experiments from the JONSWAP
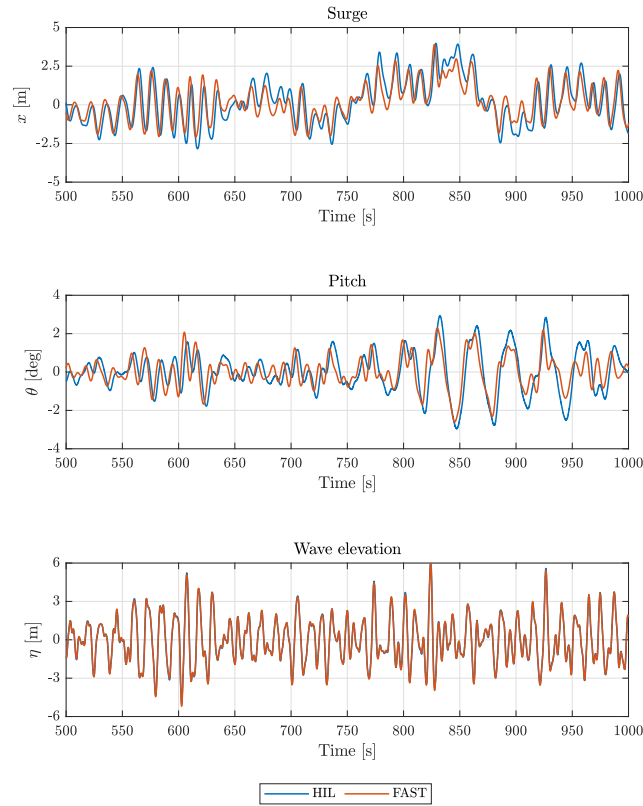
Figure 3: Platform surge and pitch response to $0°$ deg irregular waves ($H_s = 7.1$ m, $T_p = 12.1$ s) from HIL and FAST.

spectrum for a significative wave height H_s of 7.1 m and a peak period T_p of 12.1 s. Additional energy was introduced in the difference-frequency band to model second-order wave kinematics. Second-order platform forces were introduced in the HIL numerical platform model. Experimental wave loads were consistently reproduced in FAST according to the procedure described in [17] to make test and simulation results directly comparable.

The surge and pitch DOFs response in the above mentioned irregular waves and still-air resulting from HIL experiments and FAST simulations is presented in Fig. 3. The experimentally recorded wave height η is also compared to the one of the corresponding numerical simulation. The PSD of the surge and pitch response presented in Fig. 3 is shown in Fig. 4. The surge DOF dynamics as simulated in FAST matches well the experiment result, especially in the linear wave-frequency range. Some differences are instead seen for the pitch DOF: the response amplitude predicted by the FAST model is slightly lower than the experiment at the pitch mode natural frequency and above experiment in the linear-wave range. Differences in the low-frequency range could be related to the representation of platform modes damping, already evidenced by decay tests. Discrepancies in the wave-excitation range could instead be related to the hydraulic actuation system, that is responsible of introducing a non-negligible amplitude attenuation and phase loss in the platform position set-point.
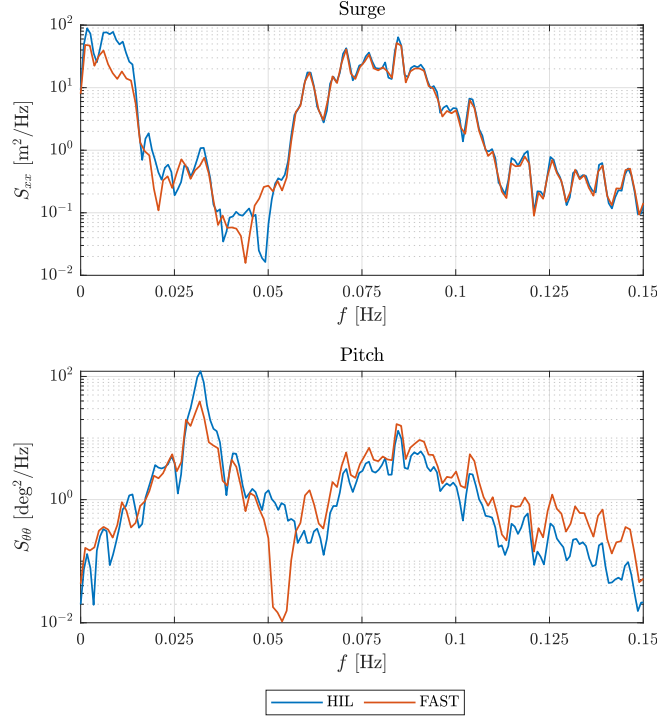
Figure 4: PSD of platform surge and pitch response to $0°$ deg irregular waves ($H_s = 7.1$ m, $T_p = 12.1$ s) from HIL and FAST.

Table 4: Wind turbine rotor speed and collective pitch angle for FAST simulations.

Operating point	U [m/s]	ω_R [rpm]	β [deg]
Below-rated	9.0	10.2	0.000
Rated	11.4	13.5	0.000
Above-rated	14.0	13.5	9.292

FAST vs HIL (wind)

Small discrepancies between still-air HIL tests and the equivalent FAST simulations confirmed the effectiveness of the procedure used to extract wind turbine loads required for the HIL force feedback. Differences between the results of experiments and simulations run in presence of wind are then expected to be mostly related to a different reproduction of rotor aerodynamics.

Decay tests and irregular wave tests already considered for the HIL methodology assessment were repeated for three wind turbine operating conditions in order to evaluate the effect of rotor loads on the platform surge and pitch response. The wind turbine controller action was excluded to lower the experiment complexity and rotor speed ω_R and collective pitch angle β were manually set for any of the three considered operating points.

FAST simulations were run according to the parameters of Tab. 4. The values of rotor speed and collective pitch angle correspond to those defined for the NREL 5MW and properly scaled according to the factors of Tab. 1. In the corresponding HIL experiments, the PoliMi wind turbine scale model rotor speed and collective pitch angle were set to the values of Tab. 5. As it can be noticed, the

8

Table 5: Wind turbine rotor speed and collective pitch angle for HIL tests at full-scale.

Operating point	U [m/s]	ω_R [rpm]	β [deg]
Below-rated	9.0	10.2	-3.500
Rated	11.4	13.5	-1.000
Above-rated	14.0	13.5	7.200

Table 6: Platform surge static translation for different wind speeds from HIL tests and FAST simulations.

Operating point	$\overline{x}$ FAST [m]	$\overline{x}$ HIL [m]
Below-rated	7.4023	5.6710
Rated	10.4486	8.5330
Above-rated	7.8481	5.9360

rotor collective pitch angle values used in HIL experiments are slightly different from those used for numerical simulations. As shown in [11], the PoliMi WTM rotor was designed to be operated at greater wind speeds than those of the present experimental campaign. At the consequent lower Reynolds numbers the thrust force predicted by the FAST/*AeroDyn 14* model is different from what is experimentally measured at the same wind speed. For this reason, the wind turbine scale model rotor collective pitch angle was adjusted to match the steady-state thrust force predicted by the numerical model.

FAST vs HIL - Free motion (wind)

Surge and pitch decay tests were repeated for the three wind turbine operating conditions, reported in Tab. 5 for the HIL experiments and in Tab. 4 for the corresponding FAST simulations, in order to evaluated how linear platform dynamics are influenced by rotor loads.

The dynamic component of surge DOF response from three surge decay tests (+5.3 m initial condition), respectively in below-rated, rated and above-rated conditions, are shown in Fig. 5, where experimental data are compared to the equivalent FAST simulations output. The steady-state surge translation for the three decay tests is reported in Tab. 6. The surge mode dynamic properties computed from the time series of Fig. 5 are reported in Tab. 7. The percent difference between linear dynamic properties form HIL tests and FAST simulations (defined as $1 - x_{FAST}/x_{HIL}$ for the generic x property) is shown in the first row of Fig. 7. The surge mode frequency, influenced by the positional component of the wind turbine rotor forcefield, is almost constant for different wind speeds both in HIL experiments and FAST simulations. Significative variations of the surge mode

Table 7: Platform surge dynamic properties for different wind speeds from HIL tests and FAST simulations.

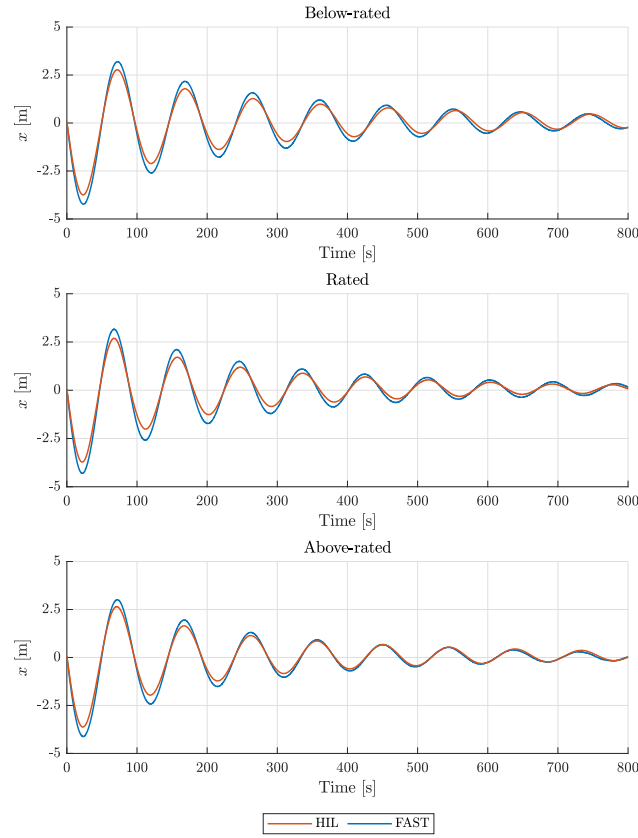|	HIL		FAST	
U [m/s]	f [Hz]	h [%]	f [Hz]	h [%]
9.0	0.0104	0.0476	0.0103	0.0527
11.4	0.0104	0.0566	0.0113	0.0575
14.0	0.0109	0.0512	0.0103	0.0575

Figure 5: Platform surge dynamic response (steady-state displacement subtracted from all signals) for a +5.3 m initial surge displacement in different wind conditions. Comparison between HIL tests and FAST simulations.

damping, proportional to the surge velocity, are seen in HIL tests but are almost absent in the output of FAST simulations. As shown in Fig. 7 the surge mode damping reproduced in HIL experiments is minimum in still-air and it is increased by rotor loads, always remaining lower than what is achieved in the corresponding FAST simulation. The HIL damping also shows a certain dependency on the mean thrust force. Its value is maximum at rated conditions, where the greatest rotor thrust force is achieved, and is almost the same at the below-rated and above-rated operating points, that are characterized by a similar steady-state thrust force.

The dynamic component of the pitch DOF response from three pitch different pitch decay tests ($+8°$ initial condition) in below-rated, rated and above-rated conditions, are shown in Fig. 6 where the response reproduced by the HIL system is compared to the output of FAST simulations. The static pitch rotation for the three decay tests is reported in Tab. 8. Small differences are seen between experimental and numerical data since the static pitch response depends only on the pitch stiffness (gravitational and buoyancy), that is the same for the HIL and FAST models, and the steady-state thrust force, more or less similar for the two systems. The wind turbine model rotor collective pitch angle was adjusted to achieve the target thrust force. The pitch mode dynamic properties obtained from the time series of Fig. 6 are resumed in Tab. 9, whereas the percent difference between the HIL and FAST values is shown in the second row of Fig. 7. The pitch mode frequency is not interested

Table 8: Platform pitch static rotation for different wind speeds from HIL tests and FAST simulations.

Operating point	$\overline{\theta}$ FAST [deg]	$\overline{\theta}$ HIL [deg]
Below-rated	3.3817	3.1501
Rated	5.4718	5.4155
Above-rated	3.6805	3.7285

Table 9: Platform pitch dynamic properties for different wind speeds from HIL tests and FAST simulations.

U [m/s]	HIL		FAST	
	f [Hz]	h [%]	f [Hz]	h [%]
9.0	0.0332	0.0751	0.0313	0.0545
11.4	0.0343	0.1027	0.0323	0.0553
14.0	0.0349	0.1039	0.0313	0.0856

by significative variations for the different wind turbine operating conditions considered here, and a similar trend is predicted by FAST simulations and HIL experiments. The still-air damping from HIL experiments increases for increasing wind speeds and is maximum in above-rated conditions. A similar trend is seen for FAST simulations but the achieved values are always lower than in the experiments.
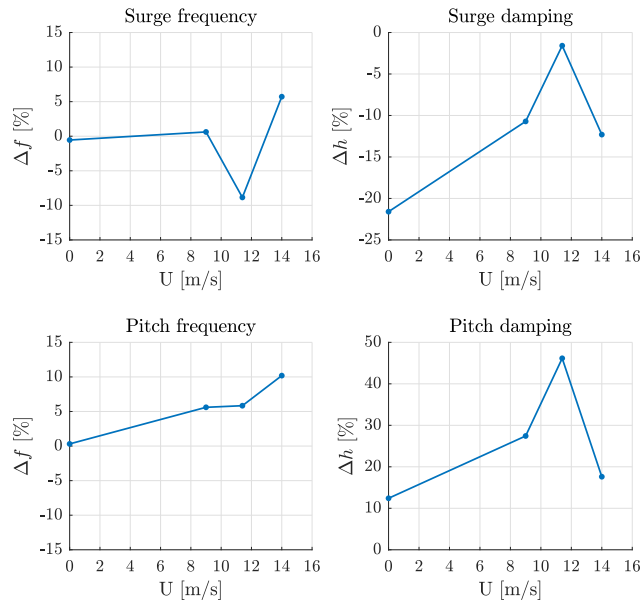

Figure 7: Percent difference between linear dynamic properties from HIL tests and FAST simulations.

FAST vs HIL - Irregular waves (wind)

The floating platform response for the different operating conditions of Tab. 5 and Tab. 4 was assessed running irregular waves from the JONSWAP spectrum (H_s of 7.1 m, T_p of 12.1 s) with 0° misalignment.
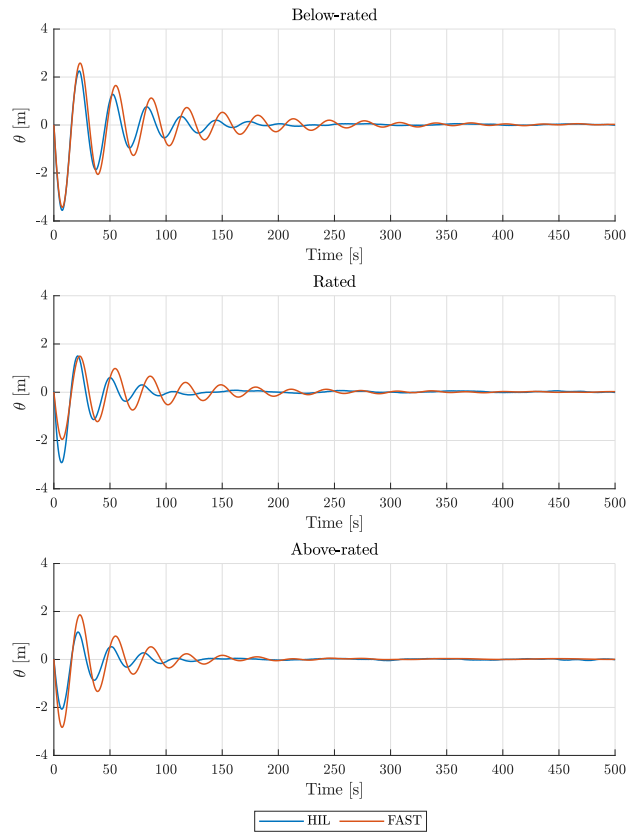
Figure 6: Platform pitch dynamic response (steady-state rotation subtracted from all signals) for a $+8°$ initial pitch rotation in different wind conditions. Comparison between HIL tests and FAST simulations.

The PSD of the platform surge and pitch DOFs response measured in HIL experiments performed in still-air, below-rated, rated and above-rated conditions is reported in Fig. 8.
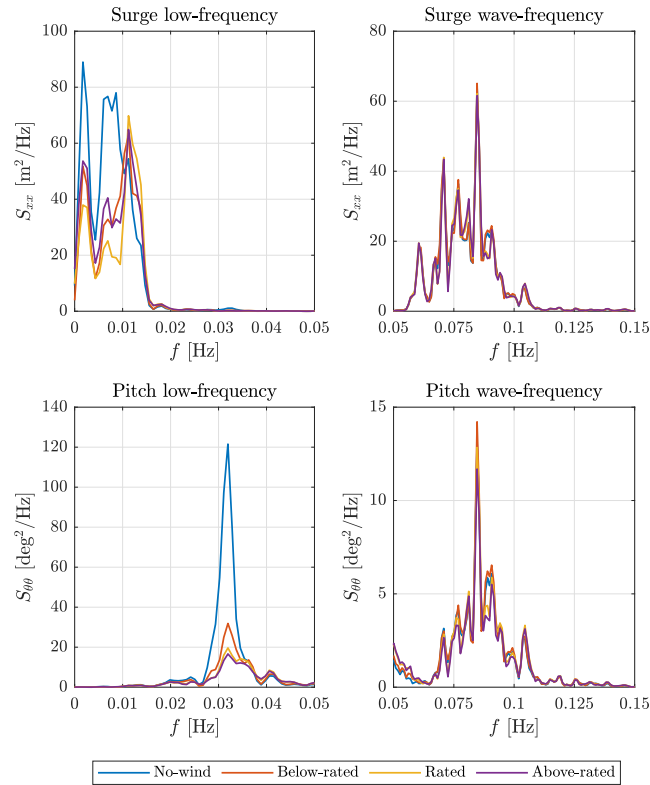
Figure 8: PSD of platform surge and pitch response to $0°$ deg irregular waves ($H_s = 7.1$ m, $T_p = 12.1$ s) in different wind conditions from HIL experiments.

In the linear wave-frequency range, the floating platform response shows a very little dependence on the operating conditions due to the strength of wave excitation loads, which effect is prevailing on rotor loads. The effect of wind turbine loads is instead visible in the low-frequency range and, in particular, at the platform modes frequencies. The surge mode frequency appears to increase when the wind turbine is rotor is spinning, but similar values are obtained for the three operating conditions considered in experimental tests. The response amplitude is almost constant for any conditions. The pitch mode frequency is not affected by wind turbine loads, whereas the response amplitude is greatly decreased in presence of wind. In particular, the minimum response amplitude is achieved in above-rated conditions and it is very similar to what is obtained for the rated wind.

The PSD of the platform surge and pitch DOFs response from FAST simulations in still-air, below-rated, rated and above-rated conditions is reported in Fig. 9.
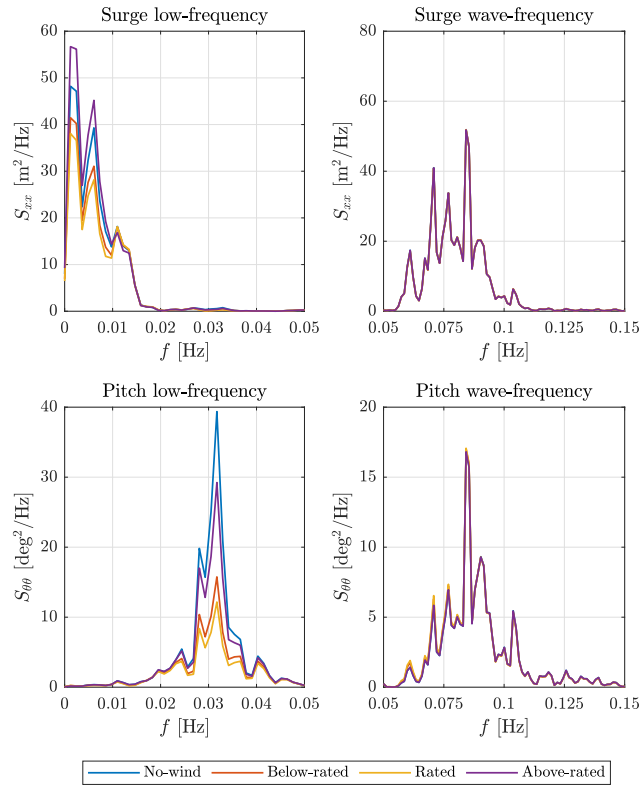
Figure 9: PSD of platform surge and pitch response to $0°$ deg irregular waves ($H_s = 7.1$ m, $T_p = 12.1$ s) in different wind conditions from FAST simulations

The difference $(S_{HIL}(f) - S_{FAST}(f))$ between the PSD of the two DOFs response from HIL tests and FAST simulations is reported in Fig. 10 Small differences are seen between experimental data and numerical results in the linear wave-frequency where, also according to the FAST model, the platform motion is not influenced by wind turbine loads. More marked differences are instead visible in the low-frequency range. The surge response at the surge mode frequency is almost constant also for the FAST model, however the surge period remains the same for any wind condition. The pitch mode frequency is not affected by the presence of wind turbine loads also in FAST simulations, whereas the pitch response amplitude is. The dependance of the latter on wind speed is however significantly less marked, with similar amplitudes reached in no-wind and above-rated conditions.
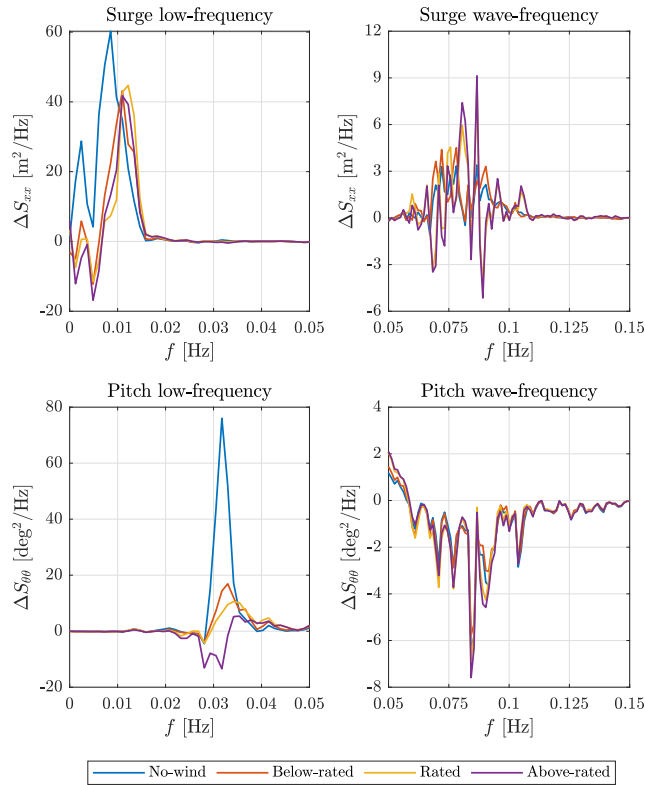
14

Figure 10: Difference between surge and pitch PSD from HIL tests and FAST simulations.

6 CONCLUSIONS

This paper presented some significative results about HIL wind tunnel tests of a DeepCwind-based floating system. In particular, the surge and pitch DOFs response was investigated for three different wind turbine operating conditions in order to understand how wind turbine loads affect the platform dynamics, and completing previous analysis of the same experimental campaign [14, 17]. Wind turbine loads have a significative influence on the platform response, particularly evident at the platform modes frequency. The effects of the positional component of the forcefield generated by the wind turbine are apparently low, with small to no variations of the platform rigid-body motion modes period, whereas the overall damping level, especially for the pitch mode, is greatly affected by the presence of wind.

The level of uncertainty of current numerical codes to predict the actual pitch aerodynamic damping still requires further research efforts [8, 12, 9, 13, 6]. A FAST model of the system object of HIL test was created and simulations equivalent to experiments were run, to assess the prediction capability of the first with respect to the effect of wind turbine loads. Numerical simulations were able to capture the same trends seen in experimental tests, with more marked differences only for what concerns the damping induced by wind turbine loads on the pitch mode.

Experimental results presented in this work directly assessed the effect of unsteady aerodynamic loads on the wind turbine response. Ongoing research by the authors is meant to compare this approach with the prediction of a simple FOWT linear model, like the one presented in [20], using as input data from unsteady loads measured in imposed motion experimental tests [9].

15

7 ACKNOWLEDGEMENTS

References

[1] Galleria del Vento Politecnico di Milano. http://www.windtunnel.polimi.it.

[2] J. Azcona, F. Bouchotrouch, M. Gonzalez, J. Garciandia, X. Munduate, F. Kelberlau, and T. A. Nygaard. Aerodynamic Thrust Modelling in Wave Tank Tests of Offshore Floating Wind Turbines Using a Ducted Fan. *Journal of Physics: Conference Series*, 524(1):012089, 2014.

[3] E. E. Bachynski, M. Thys, T. Sauder, V. Chabaud, and L. O. Sæther. Real-time hybrid model testing of a braceless semi-submersible wind turbine. part II: Experimental results. *35th International Conference on Offshore Mechanics and Arctic Engineering (OMAE) - Busan, Korea*, 6(49972), 2016. doi: 10.1115/OMAE2016-54437.

[4] C. Bak, F. Zahle, R. Bitsche, K. Taeseong, A. Yde, L. C. Henriksen, M. H. Hansen, J. P. A. A. Jose, M. Gaunaa, and A. Natarajan. The DTU 10-MW Reference Wind Turbine. *DTU Wind Energy Report*, 2013.

[5] T. Battistella, D. De Los Dolores Paradinas, A. Meseguer Urban, and R. Guanche Garcia. High Fidelity Simulation of Multi-MW Rotor Aerodynamics by Using a Multifan. *37th International Conference on Offshore Mechanics and Arctic Engineering (OMAE) - Madrid, Spain*, 10(51319), 2018. doi: 10.1115/OMAE2018-77606.

[6] I. Bayati, M. Belloli, L. Bernini, K. Boorsma, M. Caboni, M. Cormier, R. Mikkelsen, M. Serdeczny, T. Lutz, and A. Zasso. UNAFLOW project: UNsteady Aerodynamics of FLOating Wind turbines. *Journal of Physics: Conference Series*, 1037(7), 2018. http://stacks.iop.org/1742-6596/1037/i=7/a=072037.

[7] I. Bayati, M. Belloli, L. Bernini, E. Fiore, H. Giberti, and A. Zasso. On the functional design of the DTU 10MW wind turbine scale model of LIFES50+ project. *Journal of Physics: Conference Series*, 753(2), 2016. http://stacks.iop.org/1742-6596/753/i=2/a=022028.

[8] I. Bayati, M. Belloli, L. Bernini, and A. Zasso. Wind Tunnel validation of AeroDyn within LIFES50+ project: imposed Surge and Pitch tests. *Journal of Physics: Conference Series*, 753(9), 2016. http://stacks.iop.org/1742-6596/753/i=9/a=092001.

[9] I. Bayati, M. Belloli, L. Bernini, and A. Zasso. A Formulation For The Unsteady Aerodynamics Of Floating Wind Turbines, With Focus On The Global System Dynamics. *36th International Conference on Offshore Mechanics and Arctic Engineering (OMAE) - Trondheim, Norway*, 10(57786), 2017. doi: 10.1115/OMAE2017-61925.

[10] I. Bayati, M. Belloli, L. Bernini, and A. Zasso. Aerodynamic design methodology for wind tunnel tests of wind turbine rotors. *Journal of Wind Engineering and Industrial Aerodynamics*, 167:217 – 227, 2017. doi: 10.1016/j.jweia.2017.05.004.

[11] I. Bayati, M. Belloli, L. Bernini, and A. Zasso. Scale model technology for floating offshore wind turbines. *IET Renewable Power Generation*, 11(9):1120 – 1126, 2017. doi: 10.1049/iet-rpg.2016.0956.

[12] I. Bayati, M. Belloli, L. Bernini, and A. Zasso. Wind Tunnel Wake Measurements of Floating Offshore Wind Turbines. *Energy Procedia*, 137:214 – 222, 2017. doi: 10.1016/j.egypro.2017.10.375.

[13] I. Bayati, L. Bernini, A. Zanotti, M. Belloli, and A. Zasso. Experimental investigation of the unsteady aerodynamics of FOWT through PIV and hot-wire wake measurements. *Journal of Physics: Conference Series*, 1037(5), 2018. http://stacks.iop.org/1742-6596/1037/i=5/a=052024.

[14] I. Bayati, A. Facchinetti, and M. Belloli. Wind tunnel 2-DOF hybrid/HIL tests on the OC5 floating offshore wind turbine. *36th International Conference on Offshore Mechanics and Arctic Engineering (OMAE) - Trondheim, Norway*, 10(57786), 2017. doi: 10.1115/OMAE2017-61763.

[15] I. Bayati, A. Facchinetti, A. Fontanella, and M. Belloli. 6-DoF hydrodynamic modelling for wind tunnel hybrid/HIL tests of FOWT: the real-time challenge. *37th International Conference on Offshore Mechanics and Arctic Engineering (OMAE) - Madrid, Spain*, 10(51319), 2018.

[16] I. Bayati, A. Facchinetti, A. Fontanella, H. Giberti, and M. Belloli. A wind tunnel/HIL setup for integrated tests of Floating Offshore Wind Turbines. *Journal of Physics: Conference Series*, 1037(5):052025, 2018. http://stacks.iop.org/1742-6596/1037/i=5/a=052025.

[17] I. Bayati, A. Facchinetti, A. Fontanella, F. Taruffi, and M. Belloli. Analysis of FOWT dynamics in 2-DOF hybrid HIL wind tunnel experiments. *Ocean Engineering.*
forthcoming.

[18] T. Duarte. SS Fitting, Theory and User Manual.

[19] T. Duarte, M. Alves, J. Jonkman, and A. Sarmento. State-space realization of the wave-radiation force within FAST. *32nd International Conference on Offshore Mechanics and Arctic Engineering (OMAE) - Nantes, France*, 8(55423), 2013. doi: 10.1115/OMAE2013-10375.

[20] A. Fontanella, I. Bayati, and M. Belloli. Linear coupled model for floating wind turbine control. *Wind Engineering*, 42(2):115 – 127, 2018. doi: 10.1177/0309524X18756970.

[21] S. Gueydon, R. Lindeboom, W. van Kampen, and E. J. de Ridder. Comparison of two Wind Turbine Loading Emulation Techniques Based on Tests of a TLP-FOWT in Combined Wind, Waves and Current. *ASME 2018 1st International Offshore Wind Technical Conference (IOWTC) - San Francisco, CA*, 2018. doi: 10.1115/IOWTC2018-1068.

[22] J. Jonkman, S. Butterfield, W. Musial, and G. Scott. Definition of a 5-MW Reference Wind Turbine for Offshore System Development. *Technical Report NREL/TP-500-38060*, 2009.

[23] J. M. Jonkman and M. L. Buhl. FAST User's Guide. *Technical Report NREL/EL-500-38230*, 2005.

[24] A. Robertson, J. Jonkman, F. Wendt, A. Goupee, and H. Dagher. Definition of the OC5 DeepCwind Semisubmersible Floating System. *Technical Report, National Renewable Energy Laboratory*, 2014. NREL/TP-5000-60601.

[25] A. N. Robertson, F. Wendt, J. M. Jonkman, W. Popko, H. Dagher, and S. Guyedon. OC5 Project Phase II: Validation of Global Loads of the DeepCwind Floating Semisubmersible Wind Turbine. *Energy Procedia*, 137:38 – 57, 2017. 10.1016/j.egypro.2017.10.333.

[26] T. Sauder, V. Chabaud, M. Thys, E. E. Bachynski, and L. O. Sæther. Real-Time Hybrid Model Testing of a Braceless Semi-submersible Wind Turbine. Part I: the Hybrid Approach.

35th International Conference on Offshore Mechanics and Arctic Engineering (OMAE) - Busan, Korea, 6(49972), 2016. doi: 10.1115/OMAE2016-54435.

[27] G. A. M. van Kuik, J. Peinke, R. Nijssen, D. Lekou, J. Mann, J. N. Sørensen, C. Ferreira, J. W. van Wingerden, D. Schlipf, P. Gebraad, H. Polinder, A. Abrahamsen, G. J. W. van Bussel, J. D. Sørensen, P. Tavner, C. L. Bottasso, M. Muskulus, D. Matha, H. J. Lindemboom, S. Degraer, O. Kramer, S. Lenhoff, M. Sonneschein, P. E. Sørensen, R. W. Kunneke, P. E. Morthorst, and K. Skytte. Long-term research challenges in wind energy - a research agenda by the European Academy of Wind Energy. *Wind energy science*, pages 26 – 27, 2016.

[28] F. Vittori, F. Bouchotrouch, F. Lemmer, and J. Azcona. Hybrid Scaled Testing of a 5MW Floating Wind Turbine Using the SiL Method Compared With Numerical Models. *37th International Conference on Offshore Mechanics and Arctic Engineering (OMAE) - Madrid, Spain*, 10(51319), 2018. doi: 10.1115/OMAE2018-77853.